Revised Charge Equilibration Potential for Liquid Alkanes

Joseph E. Davis, G. Lee Warren, and Sandeep Patel*

Department of Chemistry and Biochemistry, University of Delaware, 238 Brown Laboratory Newark, Delaware 19716

Received: January 13, 2008; Revised Manuscript Received: March 22, 2008; In Final Form: April 2, 2008

We present a revised liquid alkane force field based on the charge equilibration formalism for incorporating electrostatic nonadditive effects arising from local polarization. The model is a revision of earlier work by Patel and Brooks, specifically addressing deficiencies in the dihedral potential, electrostatic, and Lennard−Jones (van der Waals) parameters of the force field. We discuss refinement of the alkane backbone torsion potential to match high-level ab initio relative conformational energetics for pentane, hexane, and heptane. We further discuss refinement of the electrostatic and Lennard−Jones (van der Waals) parameters to reproduce the experimental polarizability, liquid density, and vaporization enthalpy of hexane. Finally, we calculate bulk liquid properties including densities, vaporization enthalpies, self-diffusion constants, isothermal compressibilities, constant pressure heat capacities, and NMR T_1 relaxation times for a series of linear alkanes ranging from hexane to pentadecane based on the current revised model. We also compute free energies of hydration for pentane, hexane, and heptane. The revised force field offers a significantly improved overall description of these properties relative to the original parametrization. The current alkane force field represents a platform for ongoing development of a CHARMM (Chemistry at Harvard Molecular Mechanics) polarizable force field for lipids and integral membrane proteins.

I. Introduction

Alkanes, and aliphatic group containing materials in general, are an important class of fluids that are implicated in a variety of industrial and commercial processes. For example, they are used in petroleum refining and extraction, as industrial solvents, and in a wide range of commercial products including oils and cosmetics.[1,2] From a biophysical perspective, the aliphatic moiety is ubiquitous in organic and biological systems and, in this regard, commands attention in terms of an accurate representation within the context of molecular modeling and statistical mechanics based approaches to studying biophysical processes. Many such processes have been studied including protein folding, protein−protein and protein−nucleic acid interactions, and processes occurring through channels formed by integral membrane proteins.[3–8] Aliphatic groups constitute a nontrivial, low-dielectric bulk-like environment within lipid membranes; it is this environment that intimately interacts with integral membrane proteins and, in this sense, contributes in mediating myriad physiological processes.[4,9–11] Aliphatic groups are present in amino acid side chains and contribute significantly to excluded volume and hydrophobic collapse in the context of protein folding.[12] Likewise, the prevalence of this chemical moiety in carbohydrates and nucleic acids stresses the need for accurate models.[13]

Today's state-of-the-art alkane force fields, such as CHARMM,[14] GROMOS,[15–18] OPLS,[19,20] AMBER,[21,22] and others (either independent or modifications of existing potentials) have proven invaluable in describing the aliphatic moiety within the context of molecular dynamics and Monte Carlo approaches. These models have historically been developed by fitting atom-type-based parameters to reproduce experimental vaporization enthalpies, pure fluid densities (and/or vapor pressures), as well as a host of other bulk fluid and single-molecule properties.[14,19,22,23] With the recruitment of modern computational resources, solvation free energies are now assuming a more common role in the parametrization scheme, though the use of this property as a fitting criterion severely restricts the system sizes (small solvent boxes) one can use; this necessitates further care in terms of assessing the effects of simulation artifacts on the properties calculated.[24–29] Furthermore, these considerations extend to matters of transferability of such force fields outside the context of the simulation conditions under which they were developed. Despite their success, current nonpolarizable force fields suffer from their inability to account for the full dielectric response of nonpolar fluids. This is an inherent limitation associated with all current models and is intimately related to the lack of an explicit inclusion of electronic polarization which, when included, confers the ability of a dielectric response to a high-frequency oscillating field (giving rise to the optical dielectric constant ε_∞). For linear alkanes, the contribution of this component to the total dielectric constant is almost 50%; consequently, the neglect of this contribution represents a significant error in the dielectric representation of aliphatic environments, such as lipid membrane interiors. Within the Born approximation where the solvation free energy scales as $(1 - {}^1/_\varepsilon)$, a factor of 2 in the dielectric constant leads to nontrivial differences in solvation free energetics in low-dielectric media.[25]

Currently, there is ongoing effort toward developing what are considered to be the next generation of polarizable (or nonadditive) molecular force fields for modeling a wide range of materials and properties.[25,26,30] Several approaches for the inclusion of polarization are being pursued, with some of the more actively pursued being the charge equilibration or CHEQ,[31–35] Drude oscillator,[25,36–38] polarizable multipole,[39–41] and SIBFA[42,43] models. Of those mentioned, only two studies have focused on detailed properties of either a series of linear alkanes or one in particular. Vorobyov and co-workers presented a systematic study of a Drude oscillator-based model of al-

* Corresponding author. E-mail: sapatel@udel.edu.

10.1021/jp8003129 CCC: $40.75
Published on Web 06/21/2008

kanes,[25] discussing parametrization of the model as well as bulk thermodynamic, structural, dielectric, and aqueous solvation properties. Patel and Brooks[44] presented a study on a polarizable model of hexane, with specific focus on bulk liquid properties and properties of the hexane−water interface; however, in their study, Patel and Brooks did not extend their analysis to longer alkanes. Consequently, in this article, we consider the bulk liquid properties of a revised charge equilibration model for aliphatic systems (linear, saturated alkanes) as an improvement of the initial parametrization by Patel and Brooks.[44] This study will also demonstrate the degree of transferability one might expect from such models, parametrized using a single state point and a single fluid of a homologous series of related compounds. In section II, we discuss the polarizable model, issues related to its implementation and parametrization, and the computational methods used to carry out our simulations. Section III discusses the torsional potential refinement based on gas-phase torsional energetics and its relation to existing fixed-charge force fields and ab initio quantum mechanical data. The refinement of the electrostatic and van der Waals parameters is also addressed. Section IV discusses bulk liquid properties, specifically densities, vaporization enthalpies, diffusion constants, specific heats (constant pressure), isothermal compressibilities, dipole moment distributions ^{13}C NMR T_1 relaxation times, and bulk liquid structure via radial distribution functions. Solvation free energies are also discussed. Section V presents further discussion and conclusions.

II. Force Field and Simulation Methods

IIA. Force Field. The nonpolarizable CHARMM[14] force field partitions the quantum mechanical energy surface into classical terms representing bond-stretching, bond-angle bending, dihedral/torsional motion, out-of-plane distortion, dispersion interactions (Lennard-Jones), and electrostatic interactions of the pairwise Coulomb type. The polarizable model is based on the charge equilibration scheme[45] as applied to classical molecular dynamics. Although applied here in a classical potential, the formalism derives rigorously from the density functional theory of atoms in molecules[46] based on Sanderson's idea of electronegativity equalization;[47,48] polarization is effected via the migration of charge density (in the classical sense, this is condensed to a partial charge) between atomic species within a given molecule. The electronic density adjusts within the molecule so as to equalize the electrochemical potential (or equivalently, the electronegativity) at each point in the molecule. The direction and ease of flow are determined by physical properties of individual atoms as will be discussed. The reader is referred to the literature for more details.[30–33,35,45,46]

The electrostatic energy of a system of M molecules containing N atoms per molecule is:

$$E_{\text{electrostatic}} = \sum_{k=1}^{M}\sum_{i=1}^{N}\chi_{ik}Q_{ik} + \frac{1}{2}\sum_{l=1}^{M}\sum_{\alpha=1}^{N}\sum_{\beta=1}^{N}\eta_{\alpha l,\beta l}Q_{\alpha l}Q_{\beta l} + \frac{1}{2}\sum_{i=1}^{MN}{}'\sum_{j=1}^{MN}{}'\frac{Q_iQ_j}{r_{ij}} \quad (1)$$

where the χ's are atom electronegativities and the η's are the atomic hardnesses. The former quantity gives rise to a directionality of electron flow, while the latter represents a resistance, or hardness, to electron flow to or from the atom. The last term in eq 1 is a standard Coulomb interaction between sites not involved in dihedral, angle, and bonded interactions with each other (the primed notation indicates a summation only over such sites). The second term represents the local charge transfer interaction generally restricted to within a molecule (no charge transfer) or some appropriate charge normalization unit. We note that although the electronegativity and hardness follow exactly from the definitions of the electron affinity and ionization potential, and they are considered here as empirical parameters to be determined as described below. Homogeneous hardness values (for each atom type) are parametrized as discussed in Patel and Brooks.[35] Heterogeneous elements (interaction elements between different atom types) are derived from the individual atom type values based on the combining rule:[49]

$$\eta_{ij}(R_{ij},\eta_i,\eta_j) = \frac{\frac{1}{2}(\eta_i+\eta_j)}{\sqrt{1.0+\frac{1}{4}(\eta_i+\eta_j)^2R_{ij}^2}} \quad (2)$$

where R_{ij} is the separation between atoms (or more generally sites) i and j. This local screened Coulomb potential has the correct limiting behavior as $1/r$ for separations greater than about 2.5 Å. This interaction is computed for 1−2, 1−3, and 1−4 sites (sites included in bonds, angles, and dihedrals). Sites in a molecule separated by 5 or more sites interact via a Coulomb interaction; in the case of interacting molecules, the interaction between sites on different molecules is again of the Coulomb form.

Details of the parametrization of the force field are discussed elsewhere. We note here that the recent hexane parametrization of Patel and Brooks[44] (on which the current revised model is based) incorporated a reduced molecular polarizability of hexane relative to their earlier force field[35] in order to match bulk and interfacial properties; their final computed polarizability for hexane is in agreement with experimental gas phase measurements (the implications of this will be discussed below). In the present work, we will assess the quality of the polarizable alkane force field by computing the molecular polarizabilities for the series of fluids investigated.

As a final note, the charge degrees of freedom are propagated via an extended Lagrangian formulation, wherein a molecular charge neutrality constraint is imposed, thus strictly enforcing electronegativity equalization at each dynamics step. The system Lagrangian is

$$L = \sum_{i=1}^{M}\sum_{\alpha=1}^{N_i}\frac{1}{2}m_{i\alpha}\dot{r}_{i\alpha}^2 + \sum_{i=1}^{M}\sum_{\alpha=1}^{N_i}\frac{1}{2}m_{Q,i\alpha}\dot{Q}_{i\alpha}^2 - E(Q,r) - \sum_{i=1}^{M}\lambda_i\sum_{\alpha=1}^{N_i}Q_{i\alpha} \quad (3)$$

where the first two terms represent the nuclear and charge kinetic energies, the third term is the total potential energy, and the fourth term is the molecular charge neutrality constraint with λ_i, the Lagrange multiplier for each molecule, i. The fictitious charge dynamics, analogous to the fictitious wave function dynamics in Car−Parrinello (CP) type methods,[50] are determined with a fictitious charge 'mass' (adiabaticity parameter in CP dynamics). The units for this mass are (energy time^2/charge^2). The charges are propagated based on forces arising from the difference between the average electronegativity of the molecule and the instantaneous electronegativity at an atomic site.

The intramolecular components of the potential energy function (bond, angle, and torsion) are transferred from the nonpolarizable CHARMM27 (C27) force field. Direct transfer of the bond and angle components is justified based on the work

of Vorobyov et al.[25] which suggests that due to the relatively small electrostatic contribution to internal energies the impact of transferring the bond and angle terms for the polarizable model is negligible. With respect to the torsion potentials, the model of Patel and Brooks[44] also transfers the dihedral potentials from the nonpolarizable force field. The authors showed that the relative torsional energetics for the low-lying conformers thermally accessible at relevant temperatures is in acceptable agreement with current ab initio estimates. In order to gauge the soundness of this transfer for higher alkanes, we consider below the gas-phase relative conformational energetics for pentane, hexane, and heptane as a further check.

IIB. Simulation Methods. ***Bulk Liquid Simulations.*** Condensed phase molecular dynamics simulations were performed in the constant pressure and temperature (*NPT*) ensemble using the CHARMM molecular modeling package.[14] The systems consisted of 216 molecules in the case of hexane and 256 molecules for the other alkanes. All simulation lengths were 1 ns using time steps of 0.5 fs; a Verlet leapfrog integrator was used to propagate the trajectory. For each system, 10 replicate simulations were run for a total simulation time of 10 ns. System temperatures (nuclear degrees of freedom) were maintained at 298 K for all simulations of all alkane systems using the Nosé−Hoover method with a thermal piston mass of 500 (kcal/mol ps^2). Pressure was maintained at 1 atm using the Langevin piston method with a piston mass of 300 amu. Particle Mesh Ewald (PME) summation with screening parameter $\kappa = 0.320$ was used in all simulations to account for the conditionally convergent long-range electrostatic interactions; a grid spacing of 1Å was used for the fast Fourier transform (FFT) grid. Long-range van der Waals corrections were applied instantaneously in all dynamics calculations. Finally, a charge transfer constraint was enforced over the entire molecule for all systems studied (pentane to pentadecane) during all condensed phase and gas phase simulations.

Atomic charge degrees of freedom (the partial atomic charges) are propagated within an extended Lagrangian formulation. We note that the Nosé−Hoover charge dynamics does not inherently enforce strict charge neutrality (or charge conservation in general). Consequently, in each Nosé−Hoover iteration, we enforce charge neutrality for individual molecules by subtracting out the average excess charge (excess relative to the required total charge constraint) from each atom. This serves as an efficient means to ensure strict charge neutrality during the course of the simulation. As an independent test of this approach, a bond-charge increment (BCI) implementation of the charge equilibration method[51] was introduced into the CHARMM molecular modeling package and was employed for molecular dynamics simulations of the relevant systems. In the BCI approach, which has seen various earlier incarnations,[51–54] the space of independent electronic degrees of freedom is transformed from atomic-charge space to bond-charge increment space. A BCI, p_{ij}, between atoms i and j, is defined as the amount of negative charge transferred from atom i to atom j, where the directionality of this charge flow is indicated by the index order. The reader is referred to the relevant literature for more detailed discussions of such implementations and the attendant caveats and qualifications.[55] We note that the forces for the BCI variables, p_{ij}, are naturally derived as the difference in the atomic charge forces, which can be determined from the standard implementation in molecular dynamics packages. The BCI approach is attractive as it allows a natural charge neutrality constraint to high precision. For the present simulations, the average energies, densities, and charge/BCI potential energies for the BCI and Nosé−Hoover with charge neutrality enforced approaches are equivalent as is required by the correspondence of the two methods.

Gas Phase Simulations. Gas phase properties required for the calculation of derivative properties were obtained by dynamics simulations of single molecules run for 2.5 ns with 0.5 fs time steps. The single-molecule configurations were culled from various snapshots along condensed phase simulation trajectories; this ensured a more-or-less complete sampling of initial conformational states from which to run dynamics. Final results and error estimates were then obtained from averages of all such simulations.

Solvation Free Energy Calculations. The hydration free energies for each alkane model were computed by decoupling a single molecule from bulk TIP4P-FQ[33] water using thermodynamic integration (TI).[56] This decoupling process followed a two-step path in which the solute−water electrostatic terms were first decoupled before decoupling the remaining nonbonded interactions. This two-step scheme is important, since close range charge−charge interactions in the absence of Lennard-Jones repulsion can lead to a polarization catastrophe when using the charge equilibration model. By using the TI approach, we can express the total hydration free energy over both paths as

$$\Delta G^{\mathrm{TI}}_{\lambda_1+\lambda_2} = \Delta G^{\mathrm{TI}}_{\lambda_1} + \Delta G^{\mathrm{TI}}_{\lambda_2} = \int_0^1 \mathrm{d}\lambda_1 \left\langle \frac{\mathrm{d}H(\lambda_1)}{\mathrm{d}\lambda_1} \right\rangle_{\lambda_2=0} + \int_0^1 \mathrm{d}\lambda_2 \left\langle \frac{\mathrm{d}H(\lambda_2)}{\mathrm{d}\lambda_2} \right\rangle_{\lambda_1=1} \quad (4)$$

where λ_1 and λ_2 are path variables representing the electrostatic and Lennard-Jones decoupling processes, respectively, and $H(\lambda)$ is the λ-parametrized Hamiltonian of the system. Each path was divided into discrete windows corresponding to a specific value of λ over which the ensemble averages were sampled. The total free energy was then obtained by summing stepwise over all windows. Double-wide sampling was employed in each window to further reduce the sampling bias.

Along the λ_1 path, the molecule-water electrostatic interactions were decoupled by linearly scaling them to zero. Since linear scaling of the corresponding Lennard-Jones terms along the λ_2 path leads to a rapidly changing Hamiltonian near $\lambda_2 = 0$ that is difficult to adequately sample, we instead used a soft-core potential to distribute the stepwise free energy changes more evenly along the entire λ_2 path. Using the separation-shifted scaling method of Zacharias et al.,[57] the λ-dependent Lennard-Jones terms are expressed as

$$U_{\mathrm{LJ}}(\lambda_2) = (1-\lambda_2) \sum \left[\frac{A_i}{(r^2 + \delta\lambda_2)^6} - \frac{B_i}{(r^2 + \delta\lambda_2)^3} \right] \quad (5)$$

where the summation runs over all molecule−water interactions. The shift parameter δ is used to tune the potential for a given solute model and A_i and B_i are the initial atom-specific Lennard-Jones parameters controlling the nonbonded molecule−water interaction. For the alkanes presented here, it was found that shift parameters in the range of 7.0−8.0 Å^2 appeared to yield the most direct Lennard-Jones decoupling paths.

In contrast to dipole polarizable models, no additional free energy contributions from the induced dipoles are explicitly required in the present scheme, since these contributions are already implicitly included in our decoupling process. Since we do not alter the polarizability of the alkane molecule as we decouple it from the water environment, the distribution of fluctuating charges within the molecule is free to respond to

λ-dependent perturbations of the system Hamiltonian as long as the perturbations do not alter the charge constraints of the system. No difficulties are encountered in the present case, in which charge constraints are always confined to a single molecule (no intermolecule charge transfer). While convenient, this approach unfortunately does not permit an explicit decomposition of the total free energy into contributions arising solely from polarization.

Since adequate convergence of free energy calculations is a common problem[25] (especially for larger molecules) and since a single trajectory is not statistically meaningful,[58] statistical uncertainties were estimated from the standard deviation of multiple independent trajectories according to the approach previously described by Warren et al.[59]

Free energy calculations were performed under *NPT* conditions (298 K, 1 atm) in a periodically replicated cubic unit cell containing 256 TIP4P-FQ water molecules. Long-range electrostatics were computed using the smooth particle mesh Ewald (PME) method incorporating a screening parameter of 0.320, a $40 \times 40 \times 40$ grid, and fourth order B-spline interpolation. Nonbonded Lennard-Jones interactions were smoothly tapered over a 1 Å region to a cutoff of 11 Å. The leapfrog Verlet integrator with a time step of 0.5 fs was used to propagate the fluctuating charge dynamics and all fluctuating charges were thermostatted using a 1 K Nosé−Hoover bath. A charge mass of 8.9×10^{-4} ps^2/e^2 was used for all alkane charges, and a mass of 3.9×10^{-5} ps^2/e^2 was used for all TIP4P-FQ charges.

The total hydration free energy of each alkane model was determined from the average of 10 independent trajectories, each approximately 2.5 ns in length. Ten equally spaced windows, each consisting of 12.5 ps of equilibration and 37.5 ps of sampling time, were employed along the electrostatic decoupling path in addition to 12.5 ps of initial equilibration before the start of the first window; convergence of the electrostatic coupling component of the hydration free energy is relatively more robust compared to the Lennard-Jones interaction as intimated in the following. For the Lennard-Jones decoupling process, 15 nonlinearly spaced windows were employed along the λ_1 path such that the window density increased quadratically near full decoupling. This procedure allowed us to more fully sample the regions of greatest curvature in λ. Each window consisted of 25 ps of equilibration followed by a sampling time ranging from 100 to 300 ps. Prior to sampling the first window of the λ_2 path, an additional 25 ps of equilibration time was included. The total sampling time along both paths amounts to approximately 2.5 ns per trajectory and 25 ns overall. Statistical uncertainties for these calculations were computed by adding the variances from the two paths.

III. Charge Equilibration Force Field Refinement

IIIA. Torsion Potential Refinement. The refinement of the alkane torsional potential was accomplished by optimizing the parameters to reproduce conformational energy differences obtained from ab initio calculations. This procedure is described in more detail below. However, we first define the conformers being examined. For the purposes of this parametrization, we are concerned only with torsions involving the carbon backbone. By convention, we refer to the orientation of the two bonds involved in the torsion (φ_1, φ_2) as either trans (*t*), 180°, or gauche (*g*), 60°. In pentane, there are two dihedral angles involving the carbon backbone; the local energy minima occur at *tt* (180°, 180°), *tg* (180°, ± 60°), and *gg* (60°, 60°). In addition, there is another minimum referred to as *gg*$^-$, since one *gauche* orientation is opposite the other. Its orientation, however, is not (60°, −60°) as might be expected, since this places the end methyl groups very close to each other resulting in unfavorable steric interactions.[60] When relaxed, this leads to minima at (60°, −90°) and (90°, −60°). Similarly, the minima for hexane are *ttt*, *tgt*, *tgg*, *tgg*$^-$, *gtg*, and *gtg*$^-$, where the orientations of *gtg* and *gtg*$^-$ are (60°, 180°, 60°) and (60°, 180°, −60°), respectively. The *gtg* and *gtg*$^-$ conformers are not identical because of the *gauche* orientation at the one end of the chain, which results in different symmetry.

In the CHARMM force field, the torsional potential energy of a molecule is represented as a sum of contributions from each dihedral angle in the molecule.

$$V_{\text{dihedral}} = \sum_{\substack{\text{all dihedral} \\ \text{types}}} \sum_{\phi} \sum_{j} K_j[1 + \cos(n_j\phi - \delta_j)] \qquad (6)$$

The sum is carried out over all parameter sets *j* and all relevant dihedral angles φ for each dihedral type. It is desirable to optimize these parameters in order to obtain a best fit to a set of reference energy values, which in this case are ab initio conformational energies. Utilizing the approach of Klauda et al.,[61] our fitting function is defined as a weighted sum of squared differences:

$$\chi = \sum_i W_i\left(E_i^{\text{ref}} - E_i\right)^2 \qquad (7)$$

The goal is to minimize the difference between the reference energy E^{ref} and the energy E obtained using the model being optimized. Each reference data point *i* has a set of dihedral angles φ (defining the conformation), a reference energy E^{ref} (the target for the fit), and a weighting factor W. Since the parameters being optimized are applicable only to a certain torsional potential (in this case, the carbon backbone of linear alkanes), one must make use of the fact that the total potential energy can be expressed as the sum of the relevant torsional potential and any remaining energy terms. It is also necessary to take into account the fact that absolute energies cannot be compared directly between different methods. Therefore, conformational energies relative to the global energy minimum are used. For linear alkanes shorter than approximately twenty carbons,[62] the all-trans form is the global minimum. The fitting function can now be written as follows:

$$\chi = \sum_i W_i\left[\Delta E_i^{\text{ref}} - \left(\Delta E_i^0 + \Delta V_{\text{dihedral}}\right)\right]^2 \qquad (8)$$

All potential energy terms are now expressed as energies relative to the all-trans form. ΔE^0 is the relative energy without contributions from the relevant torsional potentials and $\Delta V_{\text{dihedral}}$ is obtained by making use of the fact that in the all-trans form, all carbon backbone dihedral angles are 180°:

$$\Delta V_{\text{dihedral}} = \sum_{\phi} \sum_{j} K_j[1 + \cos(n_j\phi - \delta_j)] - \sum_{\phi} \sum_{j} K_j[1 + \cos(n_j \cdot 180^\circ - \delta_j)] \qquad (9)$$

The process of minimizing this function can be greatly simplified by varying only the amplitude parameters K_j while keeping the parameters n and δ constant with respect to the optimization. This follows from the observation that the existing form and symmetry of the torsional potential are appropriate given that we introduce only small perturbations to the amplitudes. To minimize the fitting function with respect to the

TABLE 1: Torsional Parameters for the Revised Polarizable Alkane Force Field

atom types	*K (kcal/mol)*	*n*	δ (deg)
CT3-CT2-CT2-CT2	0.21974	5	0
	0.15007	4	0
	0.15460	3	180
	−0.13584	2	0
CT2-CT2-CT2-CT2	0.20715	5	0
	0.08533	4	0
	0.18205	3	180
	0.01013	2	0

parameters K_j, thus obtaining the optimal values, one only needs to solve the following set of equations:

$$\frac{\partial \chi}{\partial K_j} = \sum_k \left(\sum_i W_i C_{ij} C_{ik} \right) K_k - \sum_i W_i C_{ij} \left(\Delta E_i^{\text{ref}} - \Delta E_i^0 \right) = 0 \tag{10}$$

where

$$C_{ij} = \sum_\phi [\cos(n_j \phi - \delta_j) - \cos(n_j \cdot 180\,^\circ - \delta_j)] \tag{11}$$

In this study, ab initio conformational energies obtained from the parametrization of the C27r force field by Klauda et al.[61] were used as a reference. In that work, conformational energies calculated at the CCSD(T)/cc-PVDZ, MP2/cc-PVDZ, and MP2/cc-PVQZ levels of theory were used to obtain an extrapolated CCSD(T)/cc-PVQZ result (MP2:CC). As in that study, we take these MP2:CC results to be the reference in this reparameterization. The fitting procedure described above was carried out using 26 conformations of pentane, hexane, and heptane, which included all minima and transition states reported by Klauda et al.[61] The parameters included in the fit were only those relevant torsional potentials involving the CT3 and CT2 atom types; specifically, the $CH_2-CH_2-CH_2-CH_2$ and $CH_3-CH_2-CH_2-CH_2$ dihedral potentials were fit. Only the *K* values were fit, as described above. The *n* and δ values associated with each *K* were obtained from the revised CHARMM27 force field (C27r).[61] The geometries of each conformation (i.e., the values of the relevant dihedrals) were obtained by performing a series of minimizations and energy calculations with C27r to obtain an energy profile as a function of dihedral angle. One dihedral angle was chosen to range from −180° to 180° in increments of 1°. The other dihedrals were set to starting values of 180° or 60° (*t* and *g*, respectively) depending on the particular conformer. A first minimization was performed with all dihedral angles constrained at the starting values. All constraints were then removed except for the constraint on the dihedral of interest, i.e. the one being varied for the purpose of constructing the energy profile. A second minimization was then performed, allowing the other torsions to minimize, followed by an energy calculation. The energy of the all-trans conformer was then subtracted to obtain the relative conformational energy. These energies were plotted as a function of the dihedral of interest, and from these plots the geometries of the desired minima and maxima were obtained. The values for ΔE^0 were obtained by performing a constrained minimization and energy calculation on each conformer using a modified set of parameters in which the *K* (amplitude) for the relevant torsions were set to zero, making the total dihedral potential for that dihedral type zero.

The results of the fit are presented below. Table 1 shows the revised torsional parameters for the fluctuating charge force field. Table 2 compares the relative energies of all conformations analyzed using the original and revised polarizable force fields, the Drude oscillator model,[25] C27r, and MP2:CC. The revised polarizable model gives results consistent with the Drude and C27r models, performing better than either model in some cases. Figure 1 shows torsional profiles for pentane calculated as described above using the original charge equilibration force field, our revised force field, and C27r. From this, it can be seen more clearly that the revised force field matches the ab initio values considerably better than the original charge equilibration force field, doing about as well as or better than C27r in most cases. The plots show that those minima that were underestimated in energy by the original model come much closer to the ab initio values using the revised model.

TABLE 2: Conformational Energies (Relative to all-trans) in kcal/mol of Minima and Transition States for Pentane, Hexane, and Heptane Calculated Using the Original Charge Equilibration (CHEQ) Force Field for Hexane, the Revised Charge Equilibration Force Field, the Drude Oscillator Model, the Revised CHARMM27 Force Field (C27r), and MP2:CC (the Estimation of CCSD(T)/cc-PVQZ by Klauda et al.[a]

		original CHEQ[b]	revised CHEQ	Drude[c]	C27r[d]	MP2:CC[d]
pentane	*tg*	0.323	0.558	0.65	0.614	0.622
	tt/tg	3.354	3.019	3.11	2.946	3.200
	gg	0.482	0.892	1.16	1.170	0.985
	tg/gg	3.807	3.700	3.82	3.549	3.514
	gg$^-$	2.719	2.708	2.79	2.907	2.846
	tg/gg$^-$	3.574	3.474	3.62	3.579	3.386
hexane	*tgt*	0.477	0.569	0.61	0.578	0.600
	ttt/tgt	3.364	2.841	2.97	2.910	2.910
	tgg	0.583	0.856	1.01	1.074	0.930
	tgt/tgg	3.951	3.614	3.70	3.472	3.480
	tgg$^-$	2.954	2.736	2.70	2.782	2.740
	tgt/tgg$^-$	3.682	3.390	3.51	3.454	3.342
	gtg	0.548	1.029	1.20	1.132	1.180
	gtt/gtg	3.647	3.542	3.75	3.547	3.730
	gtg$^-$	0.694	1.148	1.21	1.280	1.230
	gtt/gtg$^-$	3.665	3.558	3.65	3.546	3.750
heptane	*tgtt*	0.445	0.537	0.53	0.552	0.560
	tttt/tgtt	3.359	2.836	2.95	2.906	2.930
	tggt	0.674	0.830	0.86	0.976	0.870
	tgtt/tggt	3.930	3.410	3.48	3.439	3.250
	tgg$^-$*t*	3.073	2.465	2.48	2.680	2.540
	tgtt/tgg$^-$*t*	3.643	3.270	3.23	3.280	3.098
	tgtg	0.687	1.029	1.10	1.081	1.140
	tgtt/tgtg	3.797	3.550	3.69	3.498	3.710
	tgtg$^-$	0.859	1.164	1.15	1.242	1.300
	tgtt/tgtg$^-$	3.817	3.568	3.61	3.508	3.730

[a] The revised polarizable model, the Drude model, and C27r were all parameterized to fit MP2:CC. [b] Reference 44. [c] Reference 25. [d] Reference 61.

One aspect worth mentioning is that the energy of the cis conformer is noticeably underestimated, more so than in other models. The issue of fitting to the cis conformer also relates to the effect of using different weighting factors on different conformers. In the study by Klauda et al.,[61] the *tg*, *gg*, and *gg*$^-$ conformers were weighted at 10, 4, and 4, respectively, while other conformations were given weights of 1. This scheme was followed in obtaining the final results for our study, with one modification. When the cis conformer was not included, its energy was underestimated. However, when it was weighted more strongly in order to fit the energy more accurately, the positions of the minima became shifted significantly. This is due to not all parameters being fit simultaneously and the fact that the fitting data does not include every possible conformation. Therefore, the cis conformer was included in the fit but given a weight of 0.1, which raised its relative energy without

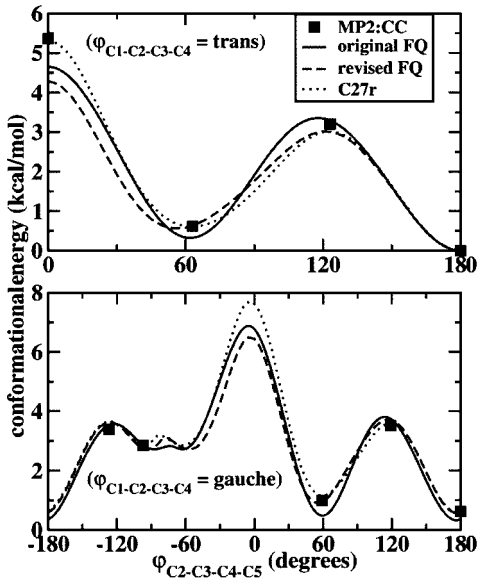

Figure 1. Conformational energy profiles as a function of dihedral angle for pentane; the original and revised polarizable models are compared to the CHARMM C27r force field and to the MP2:CC calculations by Klauda et al.

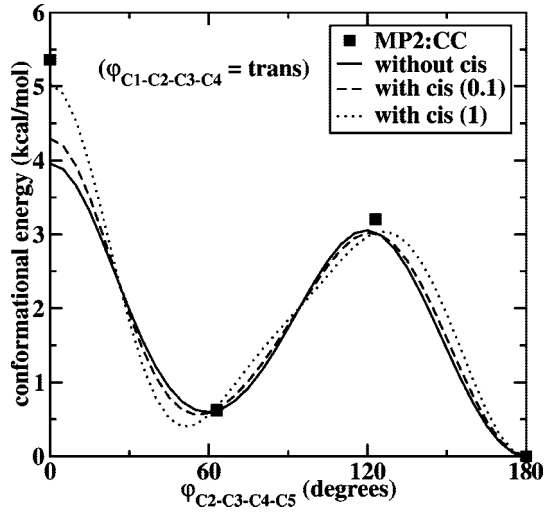

Figure 2. Conformational energy profile of pentane comparing the effects of not including the cis conformer in the fit, including the cis conformer weighted at 0.1, and including it weighted at 1.

noticeably affecting the minima. Figure 2 compares the torsional profile of pentane without the cis conformer included in the fit and with the cis conformer weighted at 0.1 and 1. Since the cis conformer is quite high in energy compared to the others, it is less likely to be significantly populated. The degree to which this is true can be estimated by calculating the Boltzmann factor, $e^{-\Delta E/kT}$, which represents the relative probability of a particular energy state being occupied. Since in this case the energies are relative to the all-trans form, the global minimum, the Boltzmann factor represents the probability that a state is occupied relative to the population of the all-trans form. Using $T = 298$ K, the Boltzmann factor calculated from the reference ab initio energy of *trans*−*cis* pentane is 0.0097% while that calculated from the revised polarizable force field is 0.061%. This indicates that the revised model does overpopulate the cis form slightly, but it is still not significantly populated compared to the minimum and therefore not thermodynamically accessible during a simulation. This suggests that those conformers that are more likely to be populated should be weighted more strongly, since

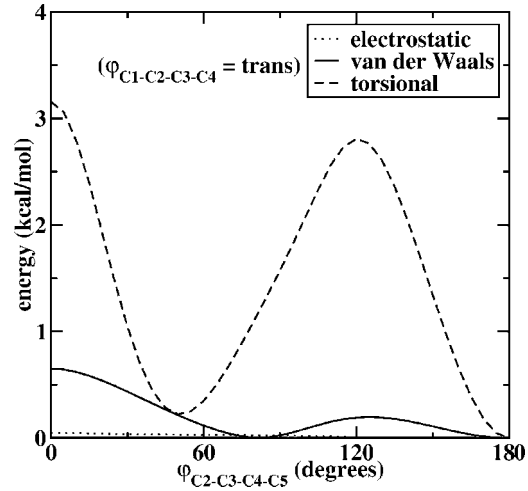

Figure 3. Torsional profile for pentane comparing the electrostatic, van der Waals, and torsional energy terms as a function of dihedral angle.

they would be more likely to be sampled in a dynamics simulation and therefore have more of an effect on properties calculated from such a simulation.

Finally, it is important to consider the degree to which other potential energy contributions, such as electrostatic and van der Waals interactions, affect the total potential energy profile as a function of dihedral angle. Optimizing the potential energy by modifying the torsional parameters is only reasonable if the torsional component is the largest contributor to the total potential energy. Otherwise, other energy contributions may require explicit optimization as a function of dihedral angle. Figure 3 shows the electrostatic, van der Waals, and torsional contributions to the conformational energy profile for pentane using the revised model. It is clear from this plot that the torsional component of the potential energy is most responsible for the overall behavior as a function of dihedral angle and that the electrostatic and van der Waals terms are small in comparison. There is a peak in the van der Waals term at the cis conformer, consistent with the cis conformer having unfavorable steric interactions. However, even that peak is not significant compared to the torsional energy. These energy terms are slightly more substantial in the C27r model (data not shown), but the torsional energy is still the main contributor. In this case, therefore, since electrostatic and van der Waals contributions are small and relatively constant compared to the torsional potential, parametrizing them with respect to the torsional profile would have little effect.

IIIB. Refinement of Electrostatic and van der Waals Parameters. ***III.B.1 Electrostatic Parameter Refinement.*** In an attempt to better reproduce bulk liquid properties of the alkanes, the electrostatic and van der Waals parameters have also been refined. For a single molecule containing N atoms, the electrostatic (eq 12) and van der Waals (eq 13) contributions to the total potential energy are expressed as follows:

$$E_{\text{elec}}(Q) = \sum_{i=1}^{N} \chi_i Q_i + \frac{1}{2}\sum_{i=1}^{N} \eta_i Q_i^2 + \sum_{i=1}^{N}\sum_{j>i}^{N} J_{ij} Q_i Q_j \quad (12)$$

$$V_{\text{LJ}}(r) = \varepsilon_{ij}\left[\left(\frac{\sigma_{ij}}{r_{ij}}\right)^{12} - 2\left(\frac{\sigma_{ij}}{r_{ij}}\right)^{6}\right] \quad (13)$$

The adjustable atomic parameters are the electronegativity χ, the hardness η, the potential well depth ε, and the van der Waals radius σ. The terms J_{ij} represent Coulomb integrals and

TABLE 3: Electrostatic and Lennard-Jones (van der Waals) Parameters for the Revised Polarizable Alkane Force Field

atom type	χ (kcal/mol e)	$\eta/2$ (kcal/mole^2)	ε (kcal/mol)	ε (1,4) (kcal/mol)	R_{min} (Å)	R_{min} (1,4) (Å)
CT2	786.076	200.697	−0.0737	−0.0067	1.9993	1.8593
CT3	788.480	229.455	−0.0737	−0.0067	1.9993	1.8593
HA2	748.509	500.471	−0.0187	n/a	1.3743	n/a
HA3	749.042	500.471	−0.0247	n/a	1.3143	n/a

TABLE 4: Molecular Polarizabilities (α) in Å^3 Calculated Using the Revised Polarizable Model for the Alkane Series Studied, along with Experimental Values of Hexane through Dodecane for Comparison

	α_{calc} (Å^3)	α_{expt} (Å^3)[a]
hexane	11.735	11.78
heptane	15.902	13.61
octane	20.890	15.44
nonane	26.726	17.36
decane	33.494	19.10
undecane	41.222	21.03
dodecane	49.987	22.75
tridecane	59.819	24.64[b]
tetradecane	70.789	26.48[b]
pentadecane	82.929	28.31[b]

[a] Reference.[69] [b] Extrapolated from a linear fit ($r^2 = 0.9999$) to the experimental data for comparison with the calculated values.

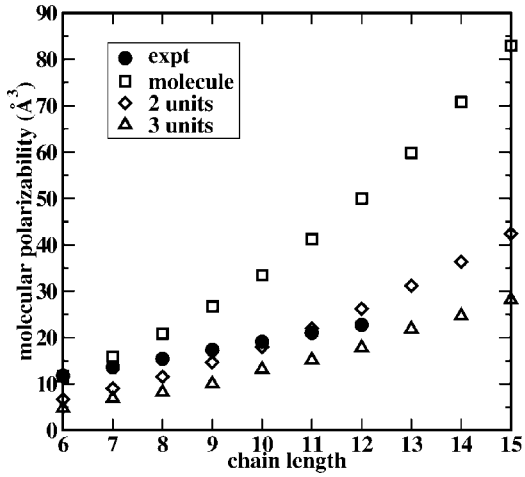

Figure 4. Molecular polarizabilities of the alkanes hexane through pentadecane using different charge-constrained units (constrained over the entire molecule, two charge-constrained units, and three charge-constrained units) compared to experiment.

in CHARMM are approximated as a function of the hardness by the atomic combination rule,[49] so these terms are implicitly parametrized along with the atomic hardnesses.

The electrostatic parameters χ and η were adjusted to reproduce the polarizability and atomic charges of hexane. For simplicity, this optimization was accomplished by scaling the parameters of all relevant atom types at once, rather than adjusting different atom types separately. Since polarizability is affected only by the hardnesses, they were first adjusted so that the computed molecular polarizability of all-*trans* hexane matched the experimental gas phase value. The all-trans form is used because one of the ultimate goals of this parametrization is the application to lipid systems, and the aliphatic groups in such systems are more extended compared to bulk liquid alkanes. Next, the electronegativities were scaled to reproduce the atomic charges originally given by CHARMM with the unmodified charge equilibration model for hexane.[44] To this end, the hardnesses of all atom types relevant to the linear alkanes were scaled from their original values by a factor of 1.325 while the electronegativities were scaled by a factor of 1.87; the final scaled values of the hardnesses and electronegativities are presented in Table 3. Computed molecular polarizabilities for the all-trans forms of hexane to pentadecane are shown in Table 4. Consistent with recent work,[54,55] the polarizabilities scale superlinearly with chain length, deviating drastically from experiment for the longer alkanes. Fully correcting this scaling problem is beyond the scope of this study; however, future work will address the issue in the context of transferability of the current model to larger macromolecular assemblies such as lipid bilayers. This shortcoming, we feel, does not preclude the application of charge equilibration models to larger molecules since one can adopt, as has been shown to be effective, smaller charge conservation groups or charge-constrained units (CCUs)[55] as a means to modulate the extent of charge transfer. As a test, polarizabilities were calculated for the alkane series with the molecules divided into two and three CCUs. These results are shown in Figure 4. It is clear that using smaller units can sufficiently damp the superlinear scaling to match the experimentally observed linear scaling. However, it is important to note that for a particular choice of CCUs, reparameterization would be necessary to reproduce the reference polarizability for a given alkane. For this parametrization, hexane was the reference and the hardnesses were fit to the polarizability calculated using a single CCU consisting of six carbons (i.e., the entire hexane molecule). Figure 4 shows that the polarizability of dodecane calculated using two units consisting of six carbons each comes reasonably close to experiment. This suggests that a limited form of transferability of the current revised parameters may be expected when applied to longer chain alkanes in which six-carbon CCUs are employed. As a test, condensed phase and gas phase simulations were performed on dodecane through pentadecane using CCUs consisting of 6 ± 1 carbons. The results and implications of this are discussed in section IVF below.

III.B.2. Refinement of Van der Waals Parameters. Next, the van der Waals parameters σ and ε were adjusted to achieve better agreement with experimental measurements of density and enthalpy of vaporization for hexane. Linear alkanes involve four atom types (CT3, HA3, CT2, and HA2) and each atom type has a set of van der Waals parameters σ and ε, for a total of eight adjustable parameters. Adjusting eight parameters to reproduce two properties is an underdetermined system, so the problem was reduced by treating the difference from the original parameters as an adjustable parameter. In other words, the size of the searchable parameter space was greatly reduced by instead considering only two adjustable parameters, $\Delta\sigma$ and $\Delta\varepsilon$, representing perturbations of the respective parameters for all atom types from their values in the original polarizable force field. For example, a $\Delta\sigma$ value of +0.01 would indicate a parameter set in which σ values for all four relevant atom types have been increased by 0.01 relative to the original polarizable force field.

To obtain data for this fit, a series of short (250 ps) simulations of bulk hexane were performed to obtain densities and enthalpies of vaporization for various arbitrary values of $\Delta\sigma$ and $\Delta\varepsilon$. Percent differences from experimental values were

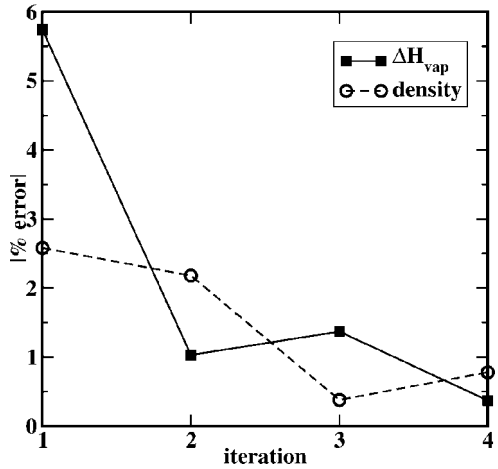

Figure 5. Absolute value of percent error from experimental vaporization enthalpy and density of hexane plotted as a function of fitting iterations; each successive iteration included more data points including the results of the previous fits.

calculated and plotted as a function of $\Delta\sigma$ and $\Delta\varepsilon$. Qualitatively, these plots suggested that each set of data could be fit to a plane, as follows:

$$d_H = a\Delta\sigma + b\Delta\varepsilon + c \quad (14)$$

$$d_\rho = p\Delta\sigma + q\Delta\varepsilon + r \quad (15)$$

where d_H is the percent difference from the experimental enthalpy of vaporization of hexane and d_ρ is the percent difference from the experimental density of hexane. The coefficients *a, b, c, p, q,* and *r* can be obtained by linear least-squares regression. Since a percent difference rather than an absolute difference is used, the models for density and vaporization enthalpy can be related directly, allowing the estimation of a parameter set in which the error in both properties is approximately minimized. The two planes of best fit intersect in a line; by determining the point at which this line intersects the plane of zero percent difference (analogous to the *xy*-plane), a unique set of parameters can be obtained from this model. It is important to note, however, that this method will not produce a true optimal parameter set, since each parameter is not varied independently. Rather, this approach is intended to refine the original force field to reproduce the reference properties (densities and vaporization enthalpies) to within an acceptable error tolerance while making the parametrization more manageable by reducing the size of the searchable space.

A bulk hexane simulation was performed with these fit parameters (as with the other data points), and the calculated density and vaporization enthalpy differed from experiment by 2.6 and 5.7%, respectively. A second fit was performed including the results of this first set of fit parameters, as well as additional data points, in order to improve the fit. This procedure was repeated a total of four times, with each successive iteration using more data points (which included the results of previous fits). As might be expected, each new set of parameters resulted in more accurate densities and vaporization enthalpies for hexane, as shown in Figure 5. The final parameter set is presented in Table 3. In the 250 ps test simulation using this parameter set, the calculated density and vaporization enthalpy differed from experiment by 0.78 and 0.37%, respectively. However, it should be noted that the quantities calculated from the production simulations (1 ns) of hexane using these parameters exhibited slightly more (but still acceptable) drift from experiment, as is shown later. This suggests that using longer simulations to obtain the data for this fitting method might improve the performance of the predicted parameters.

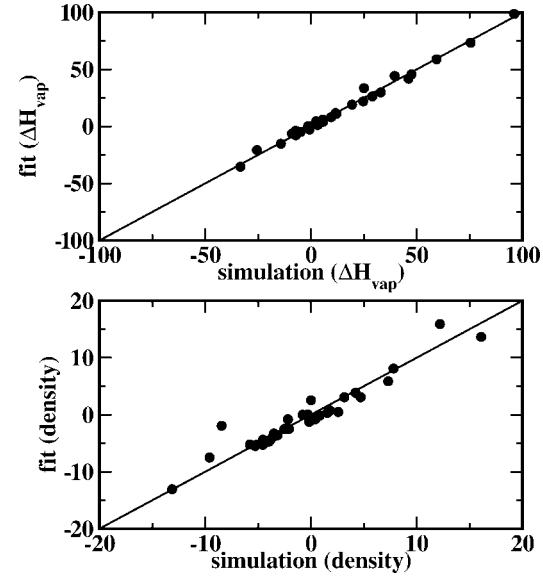

Figure 6. Predicted values of percent error (from fit to plane) plotted against the actual percent error from the experimental vaporization enthalpy (top) and density (bottom) of hexane; the line of concordance (predicted = actual) is also shown.

The quality of this fitting model can be measured by examining the root-mean-squared error from the residuals (difference between the model and the actual data). The model for the enthalpy of vaporization has a root-mean-squared error of 2.638, while the model for density has a root-mean-squared error of 1.713, where the units are percent difference from the respective experimental quantity. Another measurement of the quality of the fit is how closely the data follow the line of concordance (predicted value = reference value), shown in Figure 6. This results in a correlation coefficient (r^2) of 0.9909 for the vaporization enthalpy data and 0.9162 for the density data. Based on these statistics, we regard the fit as acceptable for the purposes of the current study.

IV. Calculated Properties of Linear Alkanes

IVA.Bulk Liquid Thermodynamic Properties. To test the performance of the revised force field, bulk liquid properties of linear alkanes ranging from hexane to pentadecane were calculated. Simulations were carried out as described in section IIB. The following properties were investigated: enthalpy of vaporization (ΔH_{vap}), density (ρ), isothermal compressibility (β_T), constant pressure heat capacity (C_P), self-diffusion constant (D), and ^{13}C NMR T_1 relaxation times. For each of these properties, averages and standard deviations were calculated from ten data points, one obtained from each replicate bulk simulation. Dipole moment distributions were calculated by averaging over a single trajectory and radial distribution functions were averaged over all replicate trajectories.

Enthalpies of vaporization were determined from the following expression:

$$\Delta H_{vap} = H_{gas} - H_{liquid} \quad (16)$$

Invoking the definition of enthalpy ($H = U + PV$) and the assumption that the vapor phase obeys the ideal gas law, eq 16 becomes

$$\Delta H_{vap} = (\langle E_{gas}\rangle + RT) - (\langle E_{liquid}\rangle + P\langle V_{liquid}\rangle) \quad (17)$$

where $\langle E_{gas}\rangle$, $\langle E_{liquid}\rangle$, and $\langle V_{liquid}\rangle$ are obtained from the average values of the relevant property in the gas and condensed phases,

and P is constant at 1 atm. The PV term accounts for volumetric expansion from liquid to gas; however, it was found to be very small in relation to the other energy terms, so it was neglected in the calculation of the vaporization enthalpy. Condensed phase densities were calculated using the average volume from the bulk simulations and the number of molecules. Isothermal compressibilities were calculated from the volume fluctuations of the bulk simulations using the following statistical mechanical expression:[63]

$$\sigma_V^2 = VN_A k_B T \beta_T \tag{18}$$

Table 5 shows the computed vaporization enthalpies, densities, and isothermal compressibilities for the liquid alkanes along with experimental data.

In keeping with the behavior of fixed-charge and alternative polarizable force fields, the revised charge equilibration model predicts bulk liquid densities to within 1.6% of experiment, vaporization enthalpies to within 1.3% across the series, and compressibilities to within 5.3%. These predictions are comparable to the Drude oscillator model for alkanes,[25] though for the longer chains the revised model exhibits slightly more drift from experiment, except in the case of compressibilities, which do not exhibit a systematic drift as a function of chain length. However, it should be noted that the Drude model was explicitly fit to reproduce these properties across the entire homologous series. There is a small, but noticeable systematic increase in the difference from experimental vaporization enthalpies as the alkane chain length increases. With the charge conservation scheme adopted here (charge constratined over the entire molecule), the larger alkanes possess a larger polarizability and hence a larger polarization energy contribution to the condensed phase cohesive energy. This leads to higher vaporization enthalpies relative to experiment. It is also important to compare the computed vaporization enthalpies to those calculated with the original polarizable force field parametrized for hexane;[44] using that model, they were predicted to within 14.2% accuracy across the series of linear alkanes, compared to 1.3% accuracy using the revised parametrization. This can be attributed to the fact that lowering the vaporization enthalpy is equivalent to lowering the difference in energy between the vapor phase and the liquid phase, thus increasing the affinity of the molecule for the vapor phase relative to the previous model. Essentially, the same effect is observed with the solvation free energies, which are addressed in section IVE.

Constant pressure heat capacities were obtained from condensed phase simulations using the approach of Jorgensen et al.,[19] in which C_P of the liquid phase is calculated from intermolecular and ideal gas contributions as

$$C^0_{P(\text{liquid})} = C_{P(\text{inter})} + C^0_{P(\text{ideal})} - R \tag{19}$$

The condensed phase trajectories were used to calculate the intermolecular contribution to C_P. For each snapshot in a given trajectory, the difference between the total energy (E_{total}) and the sum of the energies of each individual molecule (E_{intra}) was calculated to obtain the intermolecular energy (E_{inter}).

$$E_{\text{inter}} = E_{\text{total}} - E_{\text{intra}} \tag{20}$$

The fluctuations in E_{inter} were then used to calculate $C_{P(\text{inter})}$ for a given trajectory using the statistical mechanical relation:[63]

$$\sigma^2_{E_{\text{inter}}} = N_A k_B T^2 C_{P(\text{inter})} \tag{21}$$

Ideal gas heat capacities were obtained from experimental values.[64,65] Results are shown in Table 6. Like isothermal compressibilites, heat capacities are calculated from fluctuations, which can require a long simulation time to converge.[62] It is possible that even with ten 1 ns simulations, we did not obtain sufficient sampling for the fluctuations to converge. The fluctuations vary noticeably among replicate simulations, as indicated by the relatively large deviations in both the compressibilities and the heat capacities, especially in the longer alkanes. Taking this fact into consideration, our results are not unreasonable.

Self-diffusion coefficients based on periodic boundary condition (PBC) simulations were calculated from the long-time behavior of the mean square displacement of molecules using the Einstein relation:

$$D_{\text{PBC}} = \lim_{t\to\infty} \frac{1}{6t} \langle (r(t) - r(0))^2 \rangle \tag{22}$$

These values are then corrected for finite system size using a hydrodynamic model for a particle surrounded by continuum solvent of given viscosity:[61]

$$D_{\text{S}} = D_{\text{PBC}} + \frac{N_A k_B T \xi}{6\pi\eta L} \tag{23}$$

where η is the viscosity of the liquid, L is the simulation box length, and $\xi = 2.837297$. Experimental values of the viscosity[66,67] are used for the present calculations. Results are shown in Table 6. Also shown are the uncorrected values in order to demonstrate the sensitivity of final values on the finite system correction. The experimental viscosity values used for the current corrections may not correspond to the actual viscosity of the force field model, so the corrected values are a qualitative estimate of the shift in values upon correction.

IVB.Local Chain Dynamics. Local measures of dynamics along the carbon backbone are related to the ^{13}C NMR T_1 relaxation time. An accurate representation of these quantities is important in describing the local chain order and dynamics in lipid molecules, particularly in the context of a bilayer environment; moreover, as one of the ultimate applications of these force fields is for molecular modeling of solvated bilayer and integral membrane protein systems, it is important to characterize the quality of the force field with respect to this property. ^{13}C NMR T_1 relaxation times were calculated using the approach of Klauda et al.,[61] in which T_1 is calculated from the reorientation correlation functions of the CH vectors, assuming motional narrowing and an effective bond length of 1.117 Å:

$$\frac{1}{NT_1} = (1.855 \times 10^{10} s^{-2})\tau = (1.855 \times 10^{10} s^{-2}) \int_0^\infty \langle P_2(\hat{\mu}(0)\hat{\mu}(t)) \rangle \mathrm{d}t \tag{24}$$

Here, N is the number of protons bonded to the relevant carbon, τ is the rotational correlation time, $\hat{\mu}$ is the CH vector, and $P_2(x) = (3x^2 - 1)/2$, the second Legendre polynomial. Figure 7 shows the calculated T_1 values for heptane, decane, tridecane, and pentadecane together with the experimental values.[68] Our results are consistent with previous work,[25,61] in which T_1 values tended to be overestimated for smaller molecules. One may note that since the current torsional component of the alkane force field is commensurate to the CHARMM C27r force field, it is not surprising that the performance with respect to this property is consistent with that of the nonpolarizable model. This behavior suggests a more detailed investigation into the connection between local chain dynamics and the underlying energy surface in such systems.

TABLE 5: Bulk Liquid Vaporization Enthalpies (ΔH_{vap}), Densities (ρ), and Isothermal Compressibilities (β_T) Calculated Using the Revised Polarizable Alkane Force Field Compared to Experimental Values

	ΔH_{vap} (kcal/mol)		ρ (g/mL)		β_T (10^{-10} m^2/N)	
	calc	expt[a]	calc	expt[b]	calc	expt[b]
hexane	7.48 ± 0.02	7.584	0.6649 ± 0.0010	0.6606	18.11 ± 2.6	16.69
heptane	8.64 ± 0.01	8.762	0.6910 ± 0.0004	0.6795	14.20 ± 1.2	14.38
octane	9.92 ± 0.01	9.926	0.7107 ± 0.0004	0.6986	12.69 ± 0.6	12.82
nonane	11.08 ± 0.02	11.10	0.7269 ± 0.0006	0.7192	11.34 ± 1.2	11.75
decane	12.34 ± 0.01	12.28	0.7398 ± 0.0003	0.7266	10.70 ± 1.2	10.94
undecane	13.61 ± 0.02	13.49	0.7503 ± 0.0004	0.7402	10.36 ± 0.8	10.31
dodecane	14.93 ± 0.03	14.70	0.7595 ± 0.0008	0.7495	9.39 ± 0.8	9.880
tridecane	16.07 ± 0.02	15.88	0.7670 ± 0.0004	0.7564	8.92 ± 0.6	9.480
tetradecane	17.31 ± 0.03	17.00	0.7741 ± 0.0007	0.7596	8.41 ± 0.6	9.100
pentadecane	18.52 ± 0.04	18.19	0.7796 ± 0.0003	0.7685	8.27 ± 0.7	8.820
rms error	1.3%		1.6%		5.3%	

[a] Reference.[65] [b] Reference.[66]

TABLE 6: Bulk Liquid Constant Pressure Heat Capacities (C_P) and Self-Diffusion Constants (D), Both with and without the Correction for Simulation System Size Effects, Calculated Using the Revised Polarizable Alkane Force Field compared to Experimental Values

	C_P (cal/mol K)		D (10^{-5} cm^2/s)		
	calc	expt[a]	uncorrected	corrected	expt[b]
hexane	44.66 ± 0.8	47.242	3.548	4.122 ± 0.20	4.21
heptane	52.25 ± 1.0	53.690	2.864	3.269 ± 0.27	3.12
octane	60.71 ± 1.3	60.741	1.981	2.280 ± 0.07	2.356
nonane	68.75 ± 2.2	67.971	1.616	1.836 ± 0.19	1.772
decane	76.09 ± 1.2	75.160	1.146	1.316 ± 0.14	1.386
undecane	86.80 ± 1.8	82.469	1.004	1.131 ± 0.13	1.112
dodecane	96.13 ± 4.3	89.849	0.737	0.835 ± 0.15	0.871
tridecane	105.47 ± 3.4	97.249	0.753	0.830 ± 0.24	0.707
tetradecane	119.38 ± 5.6	104.79	0.569	0.629 ± 0.11	0.550
pentadecane	129.33 ± 7.2	112.32	0.382	0.432 ± 0.14	0.461
rms error	8.5%			8.2%	

[a] Reference.[65] [b] Reference[67,70]

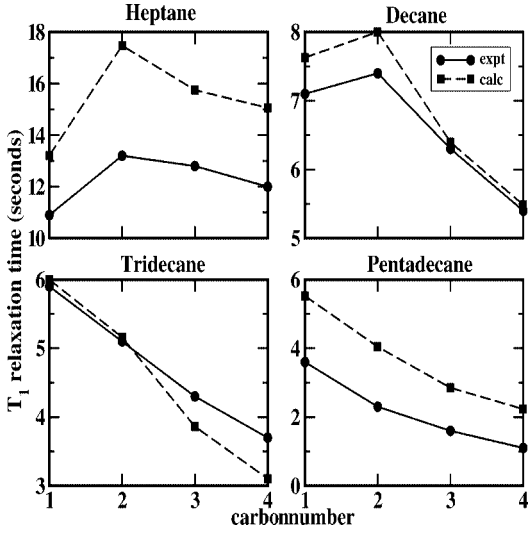

Figure 7. Calculated ^{13}C NMR T_1 relaxation times of heptane, decane, tridecane, and pentadecane compared to experiment.

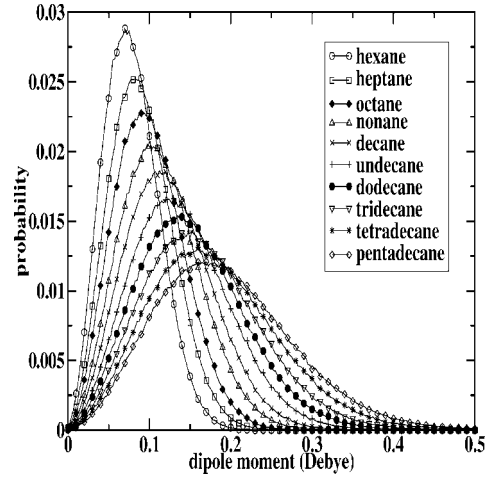

Figure 8. Induced dipole moment distributions in bulk liquid alkanes (hexane through pentadecane).

IVC.Polarization Effects. Polarizable force fields should allow one to capture the differences in electrostatic environments; this is fundamentally the strength of such models. One particular behavior exhibited with the inclusion of such physics is the shift in molecular dipole moment as a molecule transfers from the vacuum to the neat liquid. In particular, dipole moment distributions of the condensed phase simulations were calculated from the individual molecular dipole moments over all of the frames in a trajectory. The results are shown in Figure 8. Since the vacuum dipole moments of the alkanes are very small, the plot in Figure 8 is indicative of the shift from vacuum to condensed phase. Though it is difficult to gauge the accuracy of these shifts, since there is little relevant experimental data for comparison, it is evident that the longer aliphatics demonstrate a systematically larger condensed phase dipole moment shift with increasing alkane size that increases approximately linearly across the series. This trend is shown in Figure 9 and seems to indicate that the superlinear polarizability scaling observed in the gas phase does not have a significant effect on the condensed phase dipole moment shift.

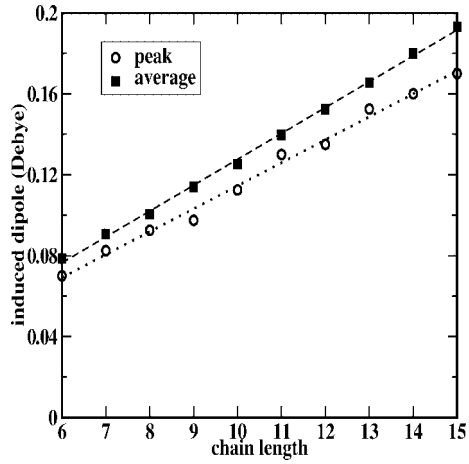

Figure 9. Peaks and averages of the induced dipole moment distributions from Figure 8 plotted as a function of alkane chain length along with lines of best fit.

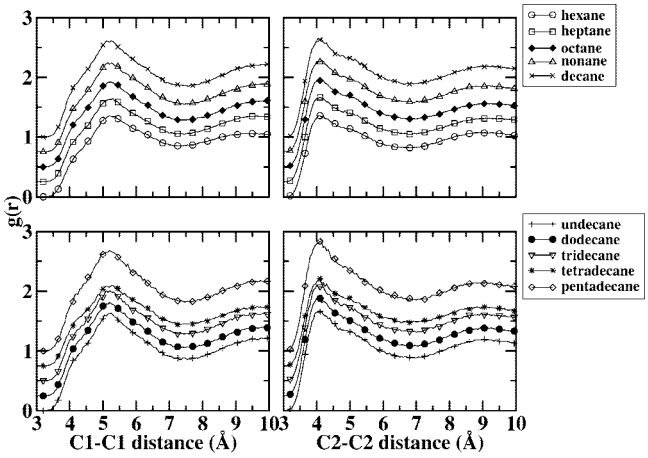

Figure 10. C1−C1 (left) and C2−C2 (right) radial distribution functions, *g(r)*, for bulk liquid hexane through decane (top) and undecane through pentadecane (bottom); for clarity, the *g(r)* have been translated vertically by multiples of 0.25.

IVD. Bulk Liquid Structure. The structure inherent in the bulk liquid phase can be represented by the radial distribution function (RDF), *g(r)*. Figure 10 shows carbon−carbon radial distribution functions calculated from the condensed phase simulations of the linear alkanes from hexane to pentadecane. The form of the function is consistent with previous work on propane[25] and is similar across the series of alkanes, indicating that the linear alkanes have similar structures in the bulk liquid phase. As one would expect, the RDFs show no dominating underlying structure in these systems but rather indicate an unstructured liquid.

IVE. Hydration Free Energies. Hydration free energies calculated using the revised polarizable model and the original model are given in Table 7. The revised model performs much better than the original polarizable model for hexane,[44] although the energies are still too favorable compared to experiment. This is consistent with results from the Drude oscillator model for alkanes.[25] The results from Table 7 also indicate an important connection between the hydration free energies and the vaporization enthalpies, which were explicitly included in the reparameterization. Specifically, the vaporization enthalpies were overestimated with the original force field; the reparameterization resulted in lower values, suggesting an increased affinity for the vapor phase. A higher affinity for the vapor phase would suggest a lower affinity for the condensed phase, resulting in a less favorable hydration free energy.

Section IIB described the methods used for constructing the window spacing used for thermodynamic integration as well as the simulation sampling times for the two portions of the calculation. It is important to note the effect of these features on the calculated free energies. The use of linear window spacing for both the Lennard-Jones and electrostatic decoupling portions of the free energy calculation gives results of 1.60 ± 0.7 kcal/mol for pentane and 1.49 ± 0.9 kcal/mol for heptane, which are less positive than the values obtained using the nonlinear spacing. This is not surprising, since a larger density of windows leads to more complete sampling in the region near full decoupling ($\lambda = 1$), which has the largest curvature in λ and a larger conformational space to be sampled. The effect of greater sampling time was also investigated. In addition to the simulations using 100 ps of sampling time per window for the Lennard-Jones decoupling portion, free energies were also calculated using 200 and 300 ps of sampling time. These results are shown in Table 7. The most noticeable effect of longer sampling time is a smaller error. However, the errors are still fairly large, so this seems to suggest that a much longer sampling time per window may be required to obtain a much smaller error. In addition, for the free energies calculated using 100 ps of sampling for the Lennard-Jones decoupling, a slight decrease with chain length was observed; this is consistent with results from the Drude oscillator model[25] but opposite to the experimentally observed trend. However, when longer sampling times (200 and 300 ps) are employed, the free energies no longer exhibit a decreasing trend and possibly suggest an increasing trend (particularly in going from pentane to hexane) that is more consistent with the experimentally observed trend. This seems to suggest that additional sampling may bring the computed free energies even more closely in line with experiment. It should also be noted that in our study, we have not used the hydration free energy as a parametrization criterion. Rather, the calculation of the solvation free energy is intended to test the performance of the revised force field as well as to quantify the effect of sampling time on error, which had been partially done in a previous study of alkanes.[25] More efficient free energy methods and longer sampling times will likely be required in order to include this property in the parametrization in the spirit of further refining the current potential. In a global sense, the current polarizable alkane model represents a rather robust parametrization with respect to the fidelity with which a broad range of condensed phase and gas phase properties are reproduced.

IVF. Effect of Smaller CCUs. To test the effect of smaller CCUs on the condensed phase properties of the longer alkanes, simulations were performed (as described in section IIB) on dodecane through pentadecane using CCUs consisting of 6 ± 1 carbons. Calculated densities and vaporization enthalpies (data not shown) were compared to those calculated using a per-molecule CCU (Table 5). The vaporization enthalpies were found to differ by less than 1% and the densities by less than 0.02%. In addition, condensed phase dipole distributions were examined as described in section IVC. These results (data not shown) indicate a very small decrease in dipole between one and two CCUs and a slightly larger decrease (~0.05 D) between one and three CCUs. It should not be surprising that using smaller CCUs results in a smaller dipole moment since, as with the polarizability scaling, smaller CCUs lead to less intramolecular charge transfer overall. Surprisingly, in our study, the observed superlinear polarizability scaling phenomenon appears

TABLE 7: Calculated Hydration Free Energies (ΔG_s) in kcal/mol of Pentane, Hexane, and Heptane Compared to the Original Polarizable Alkane Model and to Experiment[a]

	ΔG_s (original)	ΔG_s (revised)[b]	ΔG_s (revised)[c]	ΔG_s (revised)[d]	ΔG_s (expt)[e]
pentane	0.89 ± 1.1	1.73 ± 0.7	1.66 ± 0.5	1.76 ± 0.5	2.338
hexane	0.88 ± 1.0	1.72 ± 1.3	1.78 ± 0.6	1.80 ± 0.5	2.550
heptane	0.57 ± 0.7	1.62 ± 1.5	1.71 ± 0.9	1.79 ± 1.0	2.627

[a] The results from the revised model were calculated using 100, 200, and 300 ps of sampling time per window for the Lennard-Jones decoupling portion. [b] 100 ps sampling time per window for Lennard-Jones decoupling portion [c] 200 ps sampling time per window for Lennard-Jones decoupling portion [d] 300 ps sampling time per window for Lennard-Jones decoupling portion [e] Reference[71]

to have a very limited effect on the calculated bulk properties of the alkanes. However, it should be noted that the gas phase polarizabilities computed for the all-trans conformations (which exhibit the largest polarizabilities) likely do not represent the wide range of less extended conformations sampled in the condensed phase. Also, the fairly uniform molecular charge distribution in the alkanes leads to a very isotropic condensed phase electrostatic environment, yielding only weak fluctuations in the local electric fields that are largely uncorrelated with each other over the length of the alkane. This is consistent with the observation that there is little change in dipole moment distribution when pentadecane is divided into two CCUs, indicating that there are only negligible charge transfer contributions on length scales larger than eight carbons. A slightly larger change is apparent with three CCUs (consisting of five carbons each), demonstrating that charge transfer between five and eight carbons has been eliminated. These results indicate that the condensed phase environment has introduced a length scale dependent attenuation of charge transfer beyond seven or eight carbons. Thus, the condensed phase has already imposed an "effective" CCU of length seven or eight which obviates the need to manually introduce CCUs in the longer alkanes. This suggests that for longer alkanes essentially equivalent parameters can be obtained for models parametrized based either on CCUs or a constraint over the entire molecule (the latter being the approach taken in the current parametrization of the hexane model). Consequently, the model parameters introduced here are transferable between approaches employing different charge normalization schemes as long as the CCUs (such as those based on hexane) are on the order of the length scale of the condensed phase effect.

V. Conclusions

In summary, a revised polarizable force field for alkanes based on the charge equilibration formalism has been presented. Explicit fitting of the torsional parameters has allowed improved agreement with high level ab initio torsional energetics for pentane, hexane, and heptane. In addition, explicit fitting of the van der Waals parameters to the experimental vaporization enthalpy and density of hexane has allowed both of these properties to be reproduced to within less than 2% of experiment across the series of linear alkanes (hexane through pentadecane). Furthermore, the calculated solvation free energies based on thermodynamic integration molecular dynamics simulations with different sampling times for pentane, hexane, and heptane are greatly improved compared to the original polarizable model and are comparable to or better than existing force fields. Other calculated bulk liquid properties (isothermal compressibilities, self-diffusion constants, constant pressure heat capacities, and ^{13}C NMR T_1 relaxation times) are still consistent with previously reported results of the C27r and Drude oscillator models.[25,61] Isothermal compressibilities are predicted to within 5.3% of experimental values, while self-diffusion constants and constant pressure heat capacities are predicted to within 8.2 and 8.5% of experimental values, respectively. Local chain dynamics as captured by ^{13}C NMR T_1 relaxation times further validate the revised alkane torsion potentials as well as demonstrate the suitability for application of the model to lipid membrane systems. As a test of the transferability of this force field toward applications to lipid membrane systems, molecular polarizabilities were calculated using a charge-constrained unit approach[55] to show that such a method can help to correct the nonphysical superlinear scaling that is observed using a single charge constraint over the entire molecule, though reparameterization would be necessary for a specific choice of charge constraint. However, the polarizability results for dodecane using two charge-constrained units consisting of six carbons suggest that the current model could transfer acceptably to longer alkanes using units of that size. Future work in our laboratory will discuss application of the current alkane force field in conjunction with novel headgroup force fields for molecular dynamics simulations of lipid bilayers such as dimyristoylphosphatidylcholine (DMPC).

Acknowledgment. We gratefully acknowledge support from the National Institute of Health sponsored COBRE (Center of Biomedical Research) Grant Nos. P20-RR017716 at the University of Delaware (Dept. of Chemistry and Biochemistry) and P20-RR015588 (Dept. of Chemical Engineering).

References and Notes

(1) Dikshith, T. S. S.; Diwan, P. V. *Industrial Guide to Chemical and Drug Safety*; John WIley & Sons: Hyderabad, India, 2003.
(2) Borbon, A.; Fontaine, H.; Locoge, N.; Veillerot, M.; Galloo, J. C. *Atmos. Environ.* **2003**, *37*, 4051.
(3) Berneche, S.; Roux, B. *Nature* **2001**, *414*, 73.
(4) Sanderson, J. M. *Org. Biomol. Chem.* **2005**, *3*, 201.
(5) Jordan, P. C. *Biophys. J.* **1990**, *58*, 1133.
(6) Roux, B.; Allen, T.; Berneche, S.; Im, W. *Quarterly Reviews of Biophysics* **2004**, *37*, 15–103.
(7) Roux, B.; Karplus, M. *Biophys. J.* **1991**, *59*, 961.
(8) Berneche, S.; Roux, B. *Biophys. J.* **2000**, *78*, 2900.
(9) Pitman, M. C.; Grossfield, A.; Suits, F.; Feller, S. E. *J. Am. Chem. Soc.* **2005**, *127*, 4576.
(10) Pitman, M. C.; Suits, F.; Gawrisch, K.; Feller, S. E. *J. Chem. Phys.* **2005**, *122*, 244714.
(11) Sanderson, J. M.; Whelan, E. J. *Phys. Chem. Chem. Phys.* **2004**, *6*, 1012.
(12) Brylinski, M.; Konieczny, L.; Roterman, I. *Comput. Biol. Chem.* **2006**, *30*, 255.
(13) Sorin, E. J.; Rhee, Y. M.; Pande, V. S. *Biophys. J.* **2005**, *88*, 2516.
(14) Brooks, B. R.; Bruccoleri, R. E.; Olafson, B. D.; States, D. J.; Swaminathan, S.; Karplus, M. *J. Comput. Chem.* **1983**, *4*, 187.
(15) Gunsteren, W. F.v.; Daura, X.; Mark, A. E. *GROMOS force field* **1998**, *2*.
(16) Scott, W. R. P.; Hunenberger, P. H.; Tironi, I. G.; Mark, A. E.; Billeter, S. R.; Fennen, J.; Torda, A. E.; Huber, T.; Kruger, P.; Gunsteren, W. F. v. *J. Phys. Chem. A* **1999**, *103*, 3596.
(17) Schuler, L. D.; Daura, X.; Gunsteren, W. F. v. *J. Comput. Chem.* **2001**, *22*, 1205.
(18) Chandrasekhar, I.; Kastenholz, M.; Lins, R. D.; Oostenbrink, C.; Schuler, L. D.; Tieleman, D. P.; Gunsteren, W. F. v. *Eur. Biophys. J.* **2003**, *32*, 67.

(19) Jorgensen, W. L.; Maxwell, D. S.; Tirado-Rives, J. *J. Am. Chem. Soc.* **1996**, *118*, 11225.
(20) Jorgensen, W. L. *J. Am. Chem. Soc.* **1981**, *103*, 341.
(21) Case, D. A.; Thomas, E.; Cheatham, I.; Darden, T.; Gohlke, H.; Luo, R.; Merz, K. M., Jr.; Onufriev, A.; Simmerling, C.; Wang, B.; Woods, R. *J. Comput. Chem.* **2005**, *26*, 1668.
(22) Ponder, J. W.; Case, D. A. *Adv. Protein Chem.* **2003**, *66*, 27.
(23) Jorgensen, W. L. *J. Phys. Chem.* **1986**, *90*, 1276.
(24) Jorgensen, W. L.; Tirado-Rives, J. *Proc. Natl. Acad. Sci. U.S.A.* **2005**, *102*, 6665.
(25) Vorobyov, I. V.; Anisimov, V. M.; MacKerell, A. D., Jr. *J. Phys. Chem B* **2005**, *109*, 18988.
(26) MacKerell, A. D., Jr. *J. Comput. Chem.* **2004**, *25*, 1584.
(27) MacKerell, A. D., Jr.; Bashford, D.; Bellott, M.; Dunbrack, R. L., Jr.; Evanseck, J. D.; Field, M. J.; Fischer, S.; Gao, J.; Guo, H.; Ha, S.; Joseph-McCarthy, D.; Kuchnir, L.; Kuczera, K.; Lau, F. T. K.; Mattos, C.; Michnick, S.; Ngo, T.; Nguyen, D. T.; Prodhom, B.; Reiher, W. E., III; Roux, B.; Schlenkrich, M.; Smith, J. C.; Stote, R.; Straub, J.; Watanabe, M.; Wiorkiewicz-Kuczera, J.; Yin, D.; Karplus, M. *J. Phys. Chem. B* **1998**, *102*, 3586.
(28) Chen, B.; Xing, J.; Siepmann, J. I. *J. Phys. Chem.* **2000**, *104*, 2391.
(29) Caldwell, J. W.; Kollman, P. A. *J. Phys. Chem.* **1995**, *99*, 6208.
(30) Rick, S. W.; Stuart, S. J. Potentials and Algorithms for Incorporating Polarizability in Computer Simulations. In *Reviews in Computational Chemistry*; Lipkowitz, K. B., Boyd, D. B., Eds.; John Wiley and Sons: New York, 2002; pp 89.
(31) Rick, S. W.; Berne, B. J. *J. Am. Chem. Soc.* **1996**, *118*, 672.
(32) Rick, S. W.; Stuart, S. J.; Bader, J. S.; Berne, B. J. *J. Mol. Liq.* **1995**, *65/66*, 31.
(33) Rick, S. W.; Stuart, S. J.; Berne, B. J. *J. Chem. Phys.* **1994**, *101*, 6141.
(34) Patel, S.; MacKerell, A. D., Jr.; Brooks, C. L., III *J. Comput. Chem.* **2004**, *25*, 1504.
(35) Patel, S.; Brooks, C. L., III *J. Comput. Chem.* **2004**, *25*, 1.
(36) Lamoureux, G.; MacKerell, A. D.; Roux, B. *J. Chem. Phys.* **2003**, *119*, 5185.
(37) Lopes, P. E. M.; Lamoureux, G.; Roux, B.; A. D. MacKerell, J. *J. Phys. Chem. B* **2007**, *111*, 2873.
(38) Harder, E.; Anisimov, V. M.; Vorobyov, I. V.; Lopes, P. E. M.; Noskov, S. Y.; A. D. MacKerell, J.; Roux, B. *J. Chem. Theory Comput.* **2006**, *2*, 1587.
(39) Schnieders, M.; Baker, N.; Ren, P.; Ponder, J. W. *J. Chem. Phys.* **2007**, *126*, 124114.
(40) Rasmussen, T. D.; Ren, P.; Ponder, J. W.; Jensen, F. *Int. J. Quantum Chem.* **2006**, *107*, 1390.
(41) Jiao, D.; King, C.; Grossfield, A.; Darden, T.; Ren, P. *J. Phys. Chem. B* **2006**, *110*, 18553.
(42) Gresh, N. *J. Comput. Chem.* **1995**, *16*, 856.
(43) Gresh, N.; Garmer, D. R. *J. Comput. Chem.* **1996**, *17*, 1481.
(44) Patel, S.; Brooks, C. L., III *J. Chem. Phys.* **2006**, *124*, 204706.
(45) Rappe, A. K.; Goddard, W. A., III *J. Phys. Chem.* **1991**, *95*, 3358.
(46) Parr, R. G.; Yang, W. *Density-Functional Theory of Atoms and Molecules*; Oxford University Press: Oxford, 1989.
(47) Sanderson, R. T. *Chemical Bonds and Bond Energy*, 2 ed.; Academic: New York, 1976.
(48) Sanderson, R. T. *Science* **1951**, *114*, 670.
(49) Nalewajski, R. F.; Korchowiec, J.; Zhou, Z. *Int. J. Quantum Chem.* (Quantum Chemistry Symposium 22) **1988**, *22*, 349.
(50) Car, R.; Parrinello, M. *Phys. Rev. Lett.* **1985**, *55*, 2471.
(51) Banks, J. L.; Kaminski, G. A.; Zhou, R.; Mainz, D. T.; Berne, B. J.; Friesner, R. A. *J. Chem. Phys.* **1999**, *110*, 741.
(52) Kaminski, G. A.; Stern, H. A.; Berne, B. J.; Friesner, R. A.; Cao, Y. X.; Murphy, R. B.;; Zhou, R.; Halgren, T. A. *J. Comput. Chem.* **2000**, *23*, 1515.
(53) Stern, H. A.; Kaminski, G. A.; Banks, J. L.; Zhou, R.; Berne, B. J.; Friesner, R. A. *J. Phys. Chem. B* **1999**, *103*, 4730.
(54) Chelli, R.; Procacci, P.; Righini, R.; Califano, S. *J. Chem. Phys.* **1999**, *111*, 8569.
(55) Warren, G. L.; Davis, J. E.; Patel, S. *J. Chem. Phys.* **2007**, *128*, 144110.
(56) Straatsma, T. P.; McCammon, J. A. *J. Chem. Phys.* **1991**, *95*, 1175.
(57) Zacharias, M.; Straatsma, T. P.; McCammon, J. A. *J. Chem. Phys.* **1994**, *100*, 9025.
(58) Shirts, M. R.; Pitera, J. W.; Swope, W. C.; Pande, V. S. *J. Chem. Phys.* **2003**, *119*, 5740.
(59) Warren, G. L.; Patel, S. *J. Chem. Phys.* **2007**, *127*, 064509.
(60) Salam, A.; Deleuze, M. S. *J. Chem. Phys.* **2002**, *116*, 1296.
(61) Klauda, J. B.; Brooks, B. R.; MacKerell, A. D., Jr.; Venable, R. M.; Pastor, R. W. *J. Phys. Chem. B* **2005**, *109*, 5300.
(62) Thomas, L. L.; Christakis, T. J.; Jorgensen, W. L. *J. Phys. Chem. B* **2006**, *110*, 21198.
(63) Allen, M. P.; Tildesley, D. J. *Computer Simulation of Liquids*; Clarendon: Oxford, 1987.
(64) Lee, C. S.; Yoo, K.-P.; Kim, H.; Lee, H. Korea Thermophysical Properties Data Bank.
(65) Lemmon, E. W.; McLinden, M. O.; Friend, D. G. Thermophysical Properties of Fluid Systems, *NIST Chemistry WebBook, NIST Standard Reference Database No. 69*; Linstrom, P. J., Mallard, W. G., Eds.; National Institutes of Standards and Technology: Gaithersburg, MD, 2005.
(66) Lide, D. R.; Baysinger, G.; Berger, L. I.; Goldberg, R. N.; Kehiaian, H. V.; Kuchitsu, K.; Rosenblatt, G.; Roth, D. L.; Zwillinger, D. *CRC Handbook of Chemistry and Physics*, 87th ed.; CRC Press: Boca Raton, FL, 2006.
(67) Tofts, P. S.; Lloyd, D.; Clark, C. A.; Barker, G. J.; Parker, G. J. M.; McConville, P.; Baldock, C.; Pope, J. M. *Magn. Reson. Med.* **2000**, *43*, 368.
(68) Lyerla, J. R.; McIntyre, H. M.; Torchia, D. A. *Macromolecules* **1974**, *7*, 11.
(69) Miller, K. J. *J. Am. Chem. Soc.* **1990**, *112*, 8533.
(70) Douglass, D. C.; McCall, D. W. *J. Phys. Chem.* **1958**, *62*, 1102.
(71) Ben-Naim, A.; Marcus, Y. *J. Chem. Phys.* **1984**, *81*, 2016.

JP8003129